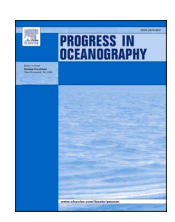
ELSEVIER

Contents lists available at ScienceDirect

Progress in Oceanography

journal homepage: www.elsevier.com/locate/pocean





Gateway to the arctic: Defining the eastern channel of the Bering Strait

Mark Zimmermann a,*, Rebecca A. Woodgate b, Megan M. Prescott c

- a National Marine Fisheries Service, NOAA, Alaska Fisheries Science Center, 7600 Sand Point Way NE, Bldg. 4, Seattle, WA 98115-6349, USA
- ^b Applied Physics Laboratory, University of Washington, 1013 NE 40th Street, Seattle, WA 98105-6698, USA
- ^c Lynker Technologies, Under contract to Alaska Fisheries Science Center, 7600 Sand Point Way NE, Bldg. 4, Seattle, WA 98115-6349, USA

ARTICLE INFO

Keywords:
USA
Alaska
Bering Strait
Cross-sectional opening
Currents
Erosion
Paleodrainage

ABSTRACT

The Bering Strait is the sole gateway and an oceanographic bottleneck for the seasonally warm and comparatively fresh and nutrient-rich Pacific waters to flow into the Arctic, melting ice, lowering salinity, and feeding bird, mammal, and fish populations. The Diomede Islands split this small strait into two main channels, both with northward flow (in the annual mean). The eastern channel, in U.S. waters, also seasonally carries the warmer, fresher Alaskan Coastal Current. Year-round in situ mooring observations (in place since 1990 with annual servicing) show a significant flow increase in the (northward) throughflow, along with seasonal and annual fluctuations. To help with measuring and modelling water flow estimates, we created the first detailed shore-toshore bathymetric surface of the Bering Strait's eastern channel, located its narrowest cross-section (1.8 km²) as occurring 5-10 km south of the moorings, and quantified the cross-section across the moorings (2.0 km²), both slightly larger than previously estimated (1.6 km²). Overlaps between older (\sim 1950) and newer (\sim 2010) bathymetry data sets identified clear areas of erosion and deposition, with much of the eastern channel having eroded by > 1 m. Since the depth is uniformly ~ 50 m across much of the eastern channel, the 1 m of erosion that we quantified would only slightly (2 %) increase the sizes of the cross-sections. Much of the seafloor is hard substrate and probably composed of cobbles, but we hypothesize that friction from strong ($\sim 1 + \text{knot}$) seafloor currents is the most likely explanation for the erosion that we observed. In softer and siltier areas, the bathymetry showed additional evidence of potential current impacts in the form of small seafloor waves (\sim 0.5 to \sim 1.0 m tall) and a shore-parallel bar offshore of Cape Prince of Wales Spit. There are large (~2 m tall) seafloor waves seaward of Cape Prince of Wales Shoal. A previously undescribed (~1 to 2 km wide, ~4 m deep) seafloor channel of unknown origin occurred along a linear north/south axis for the full 75 km extent of the bathymetric surface. The southern end of this seafloor channel was near the end of three larger seafloor channels extending westerly out of nearby Norton Sound, suggesting a common origin. These Norton Sound channels may be paleodrainages, as their eastern ends point toward Seward Peninsula inlets with large drainages where paleoglaciers were reported to have existed, but the morphology of these channels is also consistent with tidal channels.

1. Introduction

1.1. An important marine inlet

The Bering Strait is the narrow, shallow, and only inlet between the Pacific and Arctic oceans (Fig. 1). Although this strait is small, it plays an outsized role in regulating global ocean circulation by limiting the mostly northward flow of fresher and seasonally warmer Pacific waters (compared to Arctic waters), including those (>5°C warmer, >7 psu fresher; Woodgate et al., 2015) of the seasonal Alaskan Coastal Current (ACC), into the local Arctic ecosystems of the Chukchi and Beaufort seas.

This northward flow through the strait lowers salinity, melts ice, and regulates climate by enhancing stratification of both the Arctic and North Atlantic oceans (Aagaard and Carmack, 1989; Serreze et al., 2006). Due to the strait's significance, semi-permanent University of Washington (UW), Applied Physics Lab (APL) moorings have monitored water flow and physical properties across the strait since 1990 (see Woodgate, 2018 for overview). With recent lower summer Arctic ice extent (Overland et al., 2019; Kumar et al., 2020; Richter-Menge and Druckenmiller, 2020), the strait is of increasing navigational significance as the western end of a seasonally available Northwest Passage to the Atlantic Ocean (Smith and Stephenson, 2013), a shortcut blocked by

E-mail addresses: mark.zimmermann@noaa.gov (M. Zimmermann), woodgate@uw.edu (R.A. Woodgate), megan.prescott@noaa.gov (M.M. Prescott).

^{*} Corresponding author.

ice when first sought by Captain Cook in 1778 (Hayes, 2001). Despite the well-known importance of the strait, the exact size and location of the minimal cross-sectional opening across the strait have never been derived from high-quality bathymetry.

1.2. Geographic setting

Aside from the strait's oceanic importance, it occurs at or near several major geographical divisions. The strait extends 80 km from Cape Dezhnev, on the Chukotka Peninsula, the easternmost point of continental Asia, across to Cape Prince of Wales on the Seward Peninsula, the westernmost point of continental North America. Along with being the edge of a continent, Cape Prince of Wales is also the northern end of the Continental Divide of the Americas, defining Pacific and Atlantic Ocean drainages, and the western end of the Arctic Divide, defining Arctic Ocean drainages. The Big (28.8 km²) and Little Diomede (6.2 km^2) islands lie roughly in the middle of the strait and are merely \sim 4 km apart, but they are separated by the treaty boundary of the U.S.-Russia Convention Line of 1867, creating western (Russian) and eastern (U.S.) channels. The two islands are also divided by the theoretical boundary of the International Date Line. The strait is just south (~100 km) of the Arctic Circle, so it is only ice-free during the summer/ fall months, and the strait is only 12° to the east of 180° longitude, an artificial geographical construct defining the boundary between the western and eastern hemispheres. Here (reflecting limited scientific access to Russian waters), we limit our project to just the U.S. waters of the east channel of the strait, reaching eastward from Little Diomede Island to Cape Prince of Wales.

A curved spit about 0.5 to 5 km wide extends from Cape Prince of Wales for about 35 km to the NE, paralleling the mainland coastline at a distance of about 6 to 9 km and partially enclosing Lopp Lagoon (Fig. 1). Seaward of the spit, Cape Prince of Wales Shoal also extends about 35 km from the cape, and it is about 3 to 5 km wide (at depth of 10 m), making it somewhat similar in shape to the spit, but it is a little larger

and pointing in a NNE direction. Just south of the strait, about 28 km west of Cape Prince of Wales and about 15 km SE of Little Diomede Island, lies Fairway Rock, a round island, <500 m across but rising 394 ft (120.1 m) above sea level.

1.3. Ephemeral connections

During the Last Glacial Maximum (LGM), when much of the world's water was frozen in vast ice sheets and glaciers, global sea level was a 120 m lower than today (Peltier & Fairbanks, 2006). This changed the strait from being a shallow marine inlet to being the highest elevation of Beringia, a terrestrial bridge connecting Asia and North America (Hultén, 1937; Hopkins, 1967; Hopkins et al., 1982). This newly formed land linking the two continents has long been hypothesized as a migratory corridor for Paleo-Indians, but its coastal area may also have supplied a passable waterway known as the "kelp highway" (Erlandson et al., 2007). Significant glacial melt stages, and a freshwaterempowered ACC, may have created periodic hazards to travel (Royer and Finney, 2020). As the LGM waned, the melting ice raised sea levels, and Beringia shrank until it just consisted of the shallowest part of the strait between the Chukotka and Seward peninsulas. Much research has focused on when the strait reopened to oceanic water flow (e.g., Polyak et al., 2007; Pelto, 2014; Jakobsson et al., 2017; Pico et al., 2020) and how this change impacted the global climate by reconnecting the Pacific and Arctic oceans (De Boer and Nof, 2004a; De Boer and Nof, 2004b).

1.4. Charting of the strait

There is still limited published bathymetric information within the strait area despite its pre-historical importance for Paleo-Indians, millennia of summer and winter use by present Arctic Native communities, almost four centuries of Russian and European exploration, and widespread interest in its oceanographic, ecological, ethnographic, climatological, and navigational importance. In 1648, the Russian fur

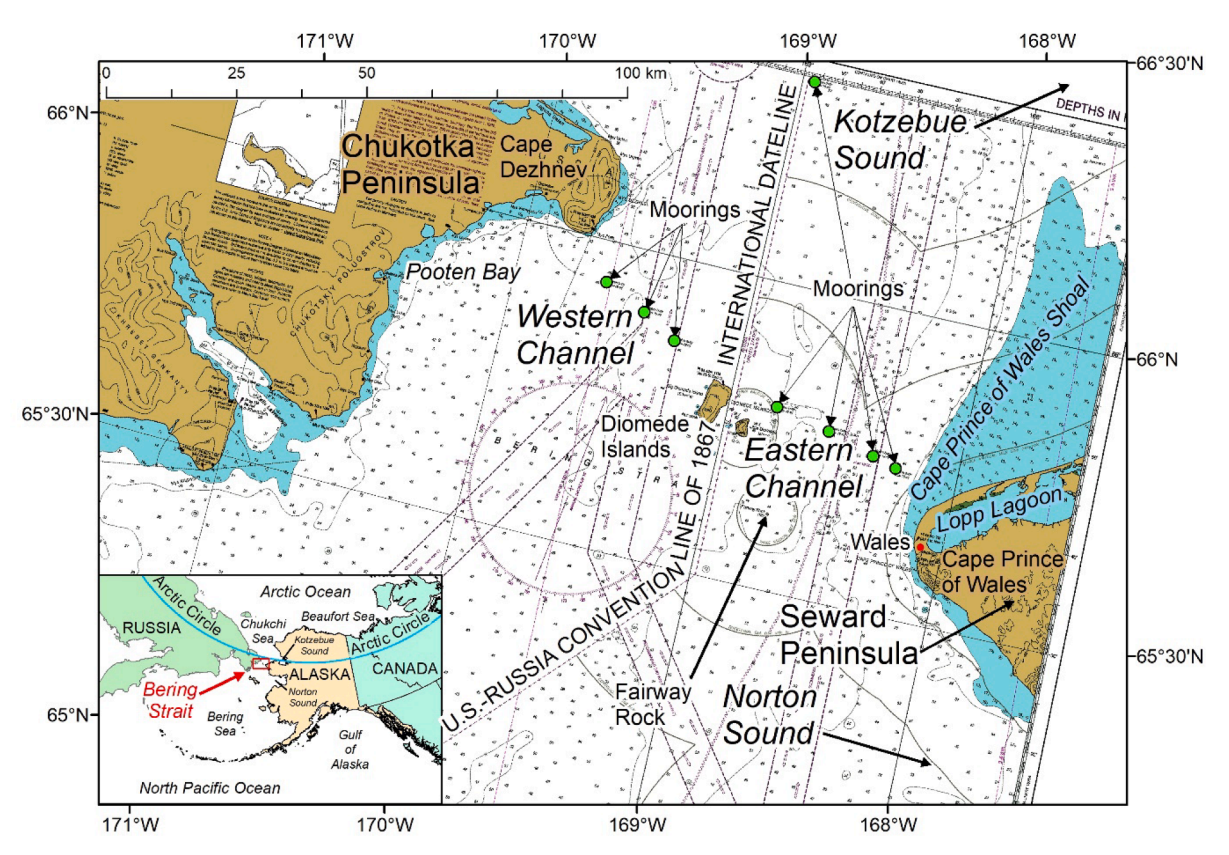


Fig. 1. Overview map of study area, based on National Ocean Service (NOS) navigational Chart 16220.

trader Semen Ivanovitch Dezhnev led an expedition that crossed from north to south through the strait, perhaps unwittingly proving that the Asia and North American continents were separated by water, but apparently no chart was produced and the significance of the discovery was not recognized (Hayes, 2001). Instead, the discovery is usually credited to the Danish Captain Vitus Bering owing to the official charts and logs from his 1728 Russian government-sponsored expedition that traveled through the strait from south to north and then back again, a feat probably aided by archived notes about Dezhnev's trip (Hayes, 2001). Because of Bering's superior documentation, the strait is named after him, while its western cape is named after Dezhnev.

The oldest U.S. navigational chart of the strait is 9380 (Scale 1:400,000) of the U.S. Coast and Geodetic Survey (USCGS), first published in June of 1900. It only shows a few soundings in the east channel of the strait but does not depict the west channel (Table 1). This USCGS chart, eventually showing about a dozen soundings along a line across the east channel by the 1967 edition, was updated to become National Ocean Service (NOS) navigational Chart 16200 in 1976, but without significant improvement of details of the east channel. NOS navigational Chart 16220 was first published in 2013 at the significantly improved scale of 1:315,350 as an updated version of a National Geospatial Intelligence Agency chart dating from 1962, adding coverage of the west channel, but still with only about a dozen soundings along lines across each channel. NOS Chart 16190 (1:100,000), first issued in 2013, still only depicts perhaps two dozen soundings along a line between Little Diomede Island and Cape Prince of Wales and also shows a largely unsounded west channel.

1.5. Hydrographic surveys

The original U.S. hydrographic surveys (1950–68) of the east channel of the strait, documented as paper records known as smooth sheets, were typically kept in archives and not widely available to the public (Table 1). The smooth sheets were often produced at large scales, such as 1:20,000, depicting thousands of soundings and were heavily subsampled to update or create the much coarser (~1:100,000) navigational charts. Digitally scanned versions of the paper smooth sheets and digitized soundings manually extracted from these digital smooth sheet images, now hosted by NCEI (The National Centers for Environmental Information: https://www.ncei.noaa.gov/maps/bathymetry/), were only made public as recently as 1996 (Wong et al., 2007). Multibeam

echosounder surveys covering most of the east channel with millions of soundings were conducted in 2010, with an additional partial coverage survey of the Cape Prince of Wales Shoal in 2015, all at a horizontal resolution of 4 m (Table 1). Extracting these older smooth sheet data, newer multibeam data, and converting them into a shore-to-shore bathymetry raster of the strait requires some GIS (Geographic Information System) expertise (Zimmermann and Benson, 2013). Thus, these more detailed bathymetry data sets have been somewhat unavailable to the research community, which instead has relied upon the widely available, but coarser, navigational charts and small-scale bathymetry compilations.

1.6. Quantifying the strait's importance

As a result of this lack of bathymetric knowledge, oceanographers have derived their own size estimates of the strait to quantify its importance for water transport. Dall (1882) provided the first summarization of anecdotal oceanographic information about the strait and, along with his own observations in 1880, established some foundational knowledge. He stated the revolutionary idea that there was a tendency for waters to flow northward rather than southward, as was generally believed at that time. He also stated that some of this northward flow was warmer and fresher than typical Bering Sea waters due to input from the discharge of local rivers, and that this river water was restricted to the surface on the east side of the eastern channel. Numerous early 20th century researchers (see within Bloom, 1964) observed Dall's freshwater oceanographic feature, and Paquette and Bourke (1974) may have coined the name of the Alaskan Coastal Current (ACC) with their publication of "Observations on the Coastal Current of Alaska" and their description of this water as "The warm coastal current of northwestern Alaska" (p. 206, Paquette and Bourke, 1974).

The name of the Alaskan Coastal Current distinguishes it from, and acknowledges a probable connection to, the freshwater runoff-powered Alaska Coastal Current in the Gulf of Alaska, originating thousands of km farther to the south than Dall realized and extending to the beginning of the Alaskan Coastal Current in the eastern Aleutian Islands. While the Alaskan Coastal Current is widely recognized as a surface current, it also extends partially to the seafloor of the eastern channel of the Bering Strait (Woodgate, 2018), much deeper than Dall thought (Dall, 1882). On Sept. 5 in 1880, Dall collected vertical temperature profiles across the entire strait, north of the Diomedes, perhaps to avoid significant

Table 1
Navigational charts, smooth sheets, and multibeam surveys of the Bering Strait. Horizontal datums: NAD27 is the North American Datum of 1927, and NAD83 is the North American Datum of 1983. Navigation methods: Shoran and Raydist were early radio beacon navigational methods, while GPS is Global Positioning System. Sounding methods: Fathometers were early singlebeam echosounders, while MB is multibeam and SB is singlebeam.

				e e		
	Year	Scale	Horizontal datum	Vessel	Navigation method	Sounding method
Navigational charts						
Chart 9380	1900	1:400,000	Unknown			
Chart 16200*	1976	1:400,000	NAD27			
Chart 16220**	2013	1:315,350	NAD83			
Chart 16190	2013	1:100,000 (inset	NAD83			
		1:20,000)				
Smooth sheets						
H07845	1950	1:20,000	NAD27	Pioneer	Shoran/Visual	Fathometer
H07849	1950	1:20,000	NAD27	Pioneer	Visual	Fathometer
H07850	1950	1:20,000	NAD27	Pioneer	Shoran	Fathometer
H08559	1960	1:100,000	NAD27	Surveyor	Raydist/Visual	Fathometer
H09020	1968	1:100,000	NAD27	Surveyor	Raydist	Fathometer
Recent multibeam						
surveys						
H12228	2010	1:40,000	NAD83	Fairweather (and launches)	GPS	MB
H12229	2010	1:40,000	NAD83	Fairweather (and launches)	GPS	MB
H12751	2015	1:40,000	NAD83	Qualifier 105 (and Autonomous Surface Vessel (ASV)-CT3)	GPS	MB/SB

^{*} Chart 16200 is formerly Chart 9380.

^{**} Chart 16220 is formerly a National Geospatial Intelligence Agency (NGA) chart dating to 1962.

lingering shore ice in Pooten Bay along the Russian coast. Dall showed what may be the first depiction of the ACC, with its surface waters by Cape Prince of Wales as much as 6.1C° warmer than on the Asian side of the strait, a difference very similar to modern-day results (e.g., Fig. 2, Woodgate et al., 2015). Using his own estimated average depth (23.5 fathoms) and approximated distance between the coasts (49.33 nmi), Dall calculated the strait's first cross-sectional area of 42,289,425 "English" ft² (3.9 km²) but neglected the impact of the shallower seafloor and land areas of the Diomedes. More recently, cross-sectional areas used in transport calculations were estimated by hand as 1.0 km² for the western channel, and 1.6 km² for the eastern channel (total 2.6 km²) from paper navigational charts (Woodgate et al., 2005, and subsequently) and are believed to have significant uncertainty (10-20 %). Representation of the strait in oceanographic models is typically poor, by virtue of having insufficient grid spacing to resolve the strait by more than a few grid points (e.g., Clement Kinney et al., 2014). No estimates exist of the cross-sectional area of the \sim 4 km wide strait between the Diomede Islands, perhaps due to its small size and lack of publicly available bathymetry data, but drop camera video (with depth sensor) demonstrated that much of this area is about 45 m deep (Fig. 3 of Cooper et al., 2019; L. W. Cooper, University of Maryland Center for Environmental Science, pers. comm., April 25, 2023).

1.7. Bathymetry compilation

Here, we combine newer, relatively comprehensive multibeam echosounder data (\sim 2010) with historical, nearshore smooth sheet data (\sim 1950) and create the first detailed shore-to-shore bathymetric surface of the eastern channel of the Bering Strait. We use this new bathymetry to derive the location and size of the minimal cross-sectional opening of

the strait's eastern channel between Cape Prince of Wales and Little Diomede Island. We calculate a second eastern channel cross-section across the annually serviced APL moorings (~4 km N of the most direct line from the north of Little Diomede to Cape Prince of Wales), where flux measurements are made, roughly along the original transect of Dall (1882). We also utilize an overlap between older (~1950) and newer (\sim 2010) bathymetry data to quantify depth change over \sim 60 years. The bathymetry, multibeam backscatter data, and sediment samples describe previously unknown eastern strait seafloor features, some extending beyond the strait into the Chukchi Sea and Norton Sound. For greater context of the seafloor features revealed within our strait bathymetry, we also plot neighboring bathymetry from the North Eastern Bering Sea Slope (Zimmermann and Prescott, 2018) and Norton Sound (Prescott and Zimmermann, 2015). Modern aerial imagery of the land and watersheds of Seward Peninsula that we derived from topography, and paleoglacier extent (Kaufman and Manley, 2004), provide additional information for seafloor feature interpretation.

2. Methods

We utilized archived digital data sets from NCEI to create a bathymetry compilation of the eastern channel of the Bering Strait from the original smooth sheets (1950–68) and recent multibeam surveys (2010 and 2015), along with some supplemental information from NOS Chart 16190 (Fig. 2). All bathymetry processing and analyses utilized ESRI's (Environmental Systems Research Institute, Redlands, CA) GIS software ArcMap (v.10.7.1) and ArcGIS Pro (v. 2.7.2).

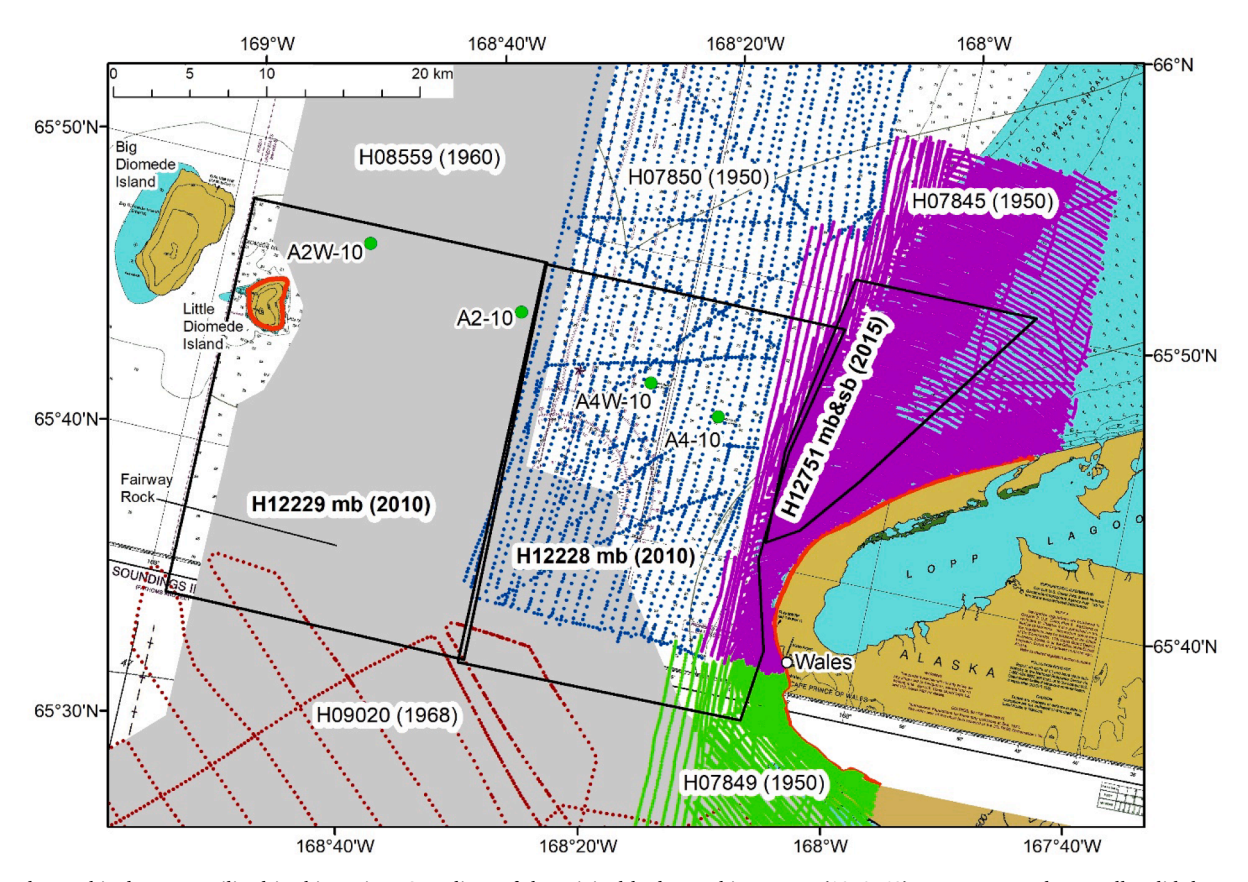


Fig. 2. Hydrographic data sets utilized in this project. Soundings of the original hydrographic surveys (1950–68) are represented as small, solid dots, with each survey a different color except for H09020, which is shown as a gray area because no soundings were available to plot. The recent (2010–15) multibeam surveys are shown as black outlines partially overlapping with the original surveys. Shorelines digitized at Cape Prince of Wales and Little Diomede Island and annotated with MHW (Mean High Water) for this survey are shown as red polylines. No high-resolution shoreline was available for Fairway Rock.

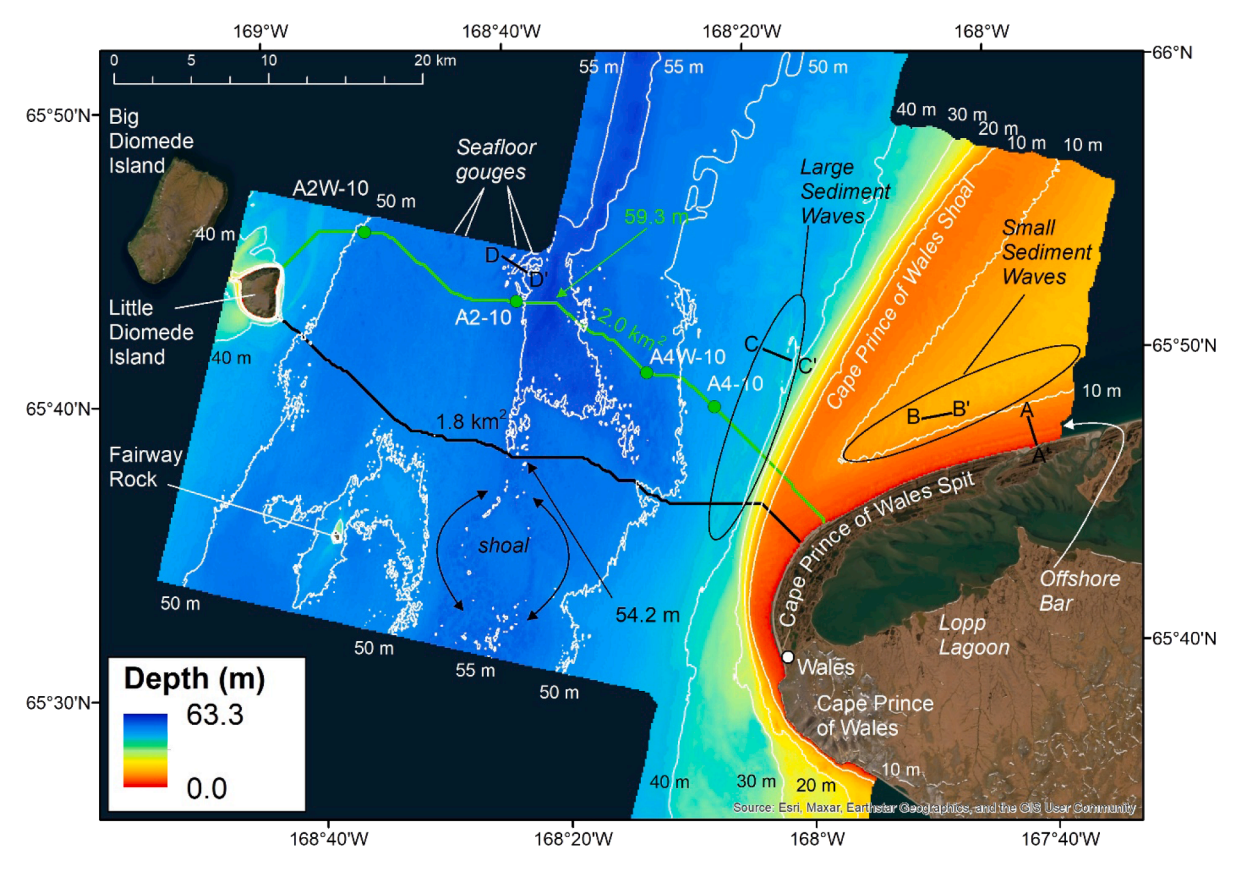


Fig. 3. Shore-to-shore bathymetry raster across the eastern channel of Bering Strait created from a combination of original (~1950) and recent (~2010) hydrographic surveys. The four UW APL historical mooring locations (A2W-10, A2-10, A4W-10, A4-10) are shown as solid green points bounded by black outlines and labeled with names. The minimal cross-sectional opening across the eastern channel (1.8 km², deepest point = 54.2 m) is indicated with a continuous black line, and the minimal opening across the moorings (2.0 km², deepest point = 59.3 m) is indicated with a continuous green line. Cross-sectional profiles, two km in length, were drawn across some small but noteworthy seafloor features (see Fig. 6). An offshore bar (cross-sectional profile A to A') occurs along the NW coast of Prince Cape of Wales Spit. Small sediment waves (B to B'), crests perpendicular to the shore occur seaward of the 10 m depth contour near Cape Prince of Wales Spit, and larger sediment waves (C to C'), crests parallel to a north–south axis, occur seaward of Cape Prince of Wales Shoal and the 40 m depth contour. Two pairs of parallel seafloor gouges occur north of mooring A2-10 and profile D to D' was drawn across the eastern pair.

2.1. Original smooth sheet surveys

The soundings from the original surveys were digitized from the scanned smooth sheets (Wong et al., 2007), but information about this digitization process is scant, and there are only minimal metadata accompanying these files at NCEI. The vessel Pioneer conducted the three smooth sheet surveys from 1950, all in the eastern portion of the eastern channel, at the relatively detailed scale of 1:20,000 (Table 1; Fig. 2). The survey of H08559 from 1960 covered the western portion of the eastern channel, ostensibly completing an original map of the strait, but the digitized data are unavailable at NCEI. The scanned smooth sheet from which we might have been able to digitize the soundings ourselves is also unavailable. It is unknown if the survey was lost, destroyed, or never completed due to technical hydrographic surveying problems reported in the survey's Descriptive Report (DR; https://data. ngdc.noaa.gov/platforms/ocean/nos/coast/H08001-H10000/H08559/ DR/). Finally, the southern area near the strait was surveyed coarsely by the Surveyor in 1968. We compared the digital sounding data of the available original surveys against the smooth sheets from which they were digitized for quality control. We found that the soundings did not need to be shifted horizontally, which was fortuitous, as navigational datum errors are common with the georegistration and digitization of older Alaska surveys (Zimmermann and Benson, 2013). Still, other editing needed to be done, such as searching for and deleting anywhere from zero (H07850), to dozens (H07849), to hundreds (H07845) of duplicate soundings that should not have been digitized from the smooth sheets. Tidal measurements for correcting soundings and

estimating the MHW (Mean High Water) value for the original smooth sheet surveys were recorded with a temporary tide station installed by the hydrographers in Lopp Lagoon for the duration of each survey.

2.2. Recent multibeam surveys

In 2010, the NOAA ship Fairweather surveyed much of the eastern channel with two multibeam surveys, and five years later, a partial coverage multibeam and singlebeam survey mapped a portion of the Cape Prince of Wales Shoal (Table 1; Fig. 2). Tidal measurements for correcting soundings from these three surveys and for estimating MHW were from the permanent Center for Operational Oceanographic Products and Services (CO-OPS), National Oceanic and Atmospheric Administration (NOAA), Red Dog Dock station, located north of Kotzebue Sound, and supplemented with temporary, local stations in the Bering Strait area. These three recent surveys resulted in overlapping 4 m horizontal resolution rasters that we combined into a single 4 m horizontal resolution composite raster by using ESRI's Mosaic to New Raster tool. This composite raster of the multibeam data extended to within ~ 100 m of Little Diomede Island but did not come within 1 km of the Cape Prince of Wales, leaving a large nearshore gap. We used this composite 4 m raster for the depth change comparison to smooth sheet soundings.

The recent multibeam surveys collected a total of 20 sediment samples with unspecified equipment, but presumably with bottom grabs rather than corers. Verbal descriptions appear to have been assigned to the sediment samples visually at sea rather than in a laboratory.

Backscatter was recorded for multibeam surveys H12228 and H12229 at a variety of horizontal resolutions ranging from ~ 1 m to ~ 20 m, which we combined using ESRI's Mosaic to New Raster tool at a horizontal resolution of 1 m to preserve all original resolutions and maintain gaps in coverage.

2.3. Shorelines

We digitized as polylines the shorelines from H07845 and H07849 at Cape Prince of Wales and annotated them with MHW values (-0.3 feet or $-0.091\,$ m) from the DRs from those surveys to complete the eastern inshore area of the eastern strait (Fig. 2). None of the available smooth sheets depicted the Little Diomede Island shoreline; therefore, we digitized it from the 1:20,000 inset of the island on NOS Chart 16190, also assigning it the same MHW value as for the eastern shore of the strait. While it would have been preferable to digitize shorelines from the more recent multibeam surveys, smooth sheets were not produced, and MHW estimates were not published in those DRs. We found no reliable shoreline of Fairway Rock, so we used the edges of multibeam survey H12229 around this small island to define the extent of our final bathymetry surface.

2.4. Shore-to-shore raster

To make a complete shore-to-shore bathymetry raster across the eastern channel, we combined points or individual soundings from the original smooth sheets, the recent multibeam surveys, and our digitized shoreline data. The smooth sheet soundings, partially filling the $> 1~\rm km$ nearshore multibeam gap at Cape Prince of Wales but older and regarded as lower quality, were edited to remove any overlap with the newer, higher quality composite 4 m multibeam raster. The center of each raster cell of the composite multibeam 4 m raster was converted into a point and annotated with the same depth value as its parent raster cell, creating millions of points equally spaced 4 m apart. The vertices of the shoreline polylines were converted into points and annotated with the

elevation of MHW. A TIN (Triangulated Irregular Network) was created from the non-overlapping smooth sheet soundings, raster points, and shoreline vertices, and then the TIN was converted into a shore-to-shore bathymetry raster of 100 m horizontal resolution (Fig. 3) with ESRI's Conversion tool.

2.5. Minimum cross-sections

We used ESRI's Cost Connect tool to derive the path of the minimum cross-sectional opening across the eastern channel from the 100 m shore-to-shore bathymetry raster (Fig. 3). We also used Cost Connect to derive the path of a second minimal opening through the historical locations of the four APL moorings (of 2007–2013, Woodgate et al., 2015) (Fig. 3). The polyline of both minimal cross-sections was used to extract depth values from the 100 m shore-to-shore raster to determine the deepest raster cell of each path. The curved and straight lengths of each cross-section were also derived.

While most researchers have already noted that the strait is small, we wondered if it was unusually shallow for its cross-sectional area or unusually narrow for its depth. There are limited data available to test this question, so we plotted the maximum depth versus cross-sectional area for other recently analyzed inlets in Alaska, such as the passes of the Aleutian Islands (Zimmermann and Prescott, 2021a), False Pass (Zimmermann and Prescott, 2021b), and Shelikof Strait (Zimmermann et al., 2019b) as a reference (Fig. 4).

2.6. Depth change over time

We used ESRI's Extraction tool to apply a depth from the 4 m multibeam composite raster to each smooth sheet sounding where the original and recent bathymetry data sets overlapped. This yielded a single multibeam depth value for each smooth sheet sounding. New depths subtracted from old depths determined depth change over time, with negative values indicating erosion and positive values indicating deposition.

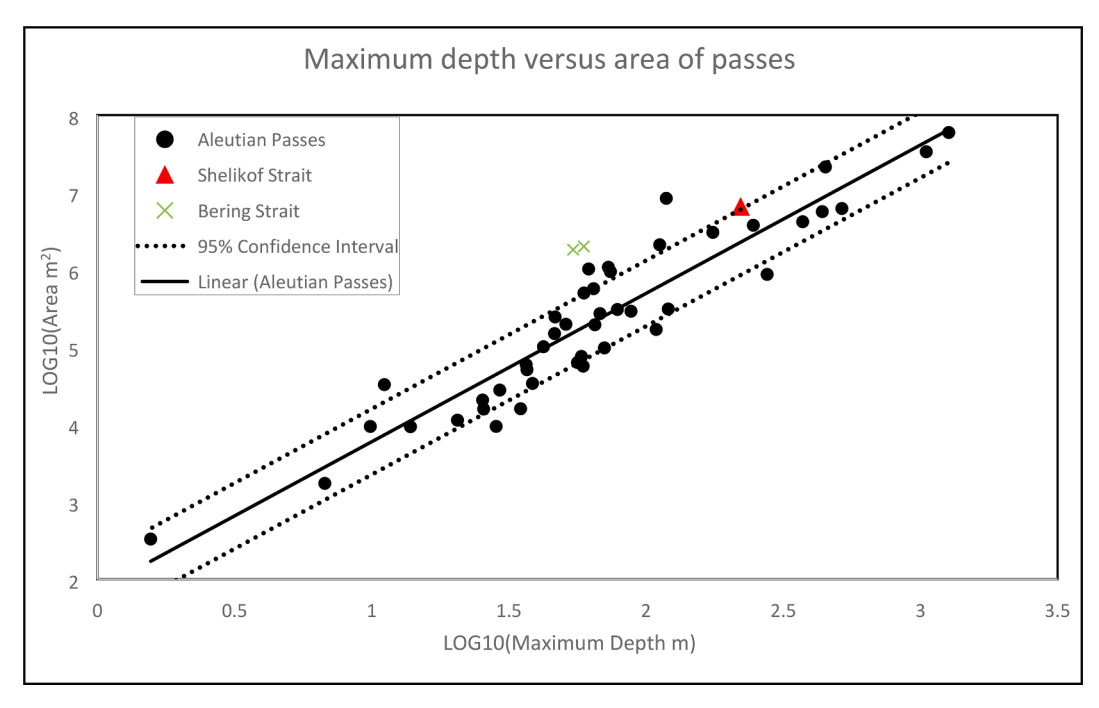


Fig. 4. Comparison between the base-10 log of maximum depth (found on the path of minimal cross-sectional area) of passes/inlets and the base-10 log of their minimal cross-sectional areas for Alaskan passes (as per legend). The linear regression was run through only the Aleutian Passes (Zimmermann and Prescott, 2021a), False Pass (both the northern False Pass inlet and southern Isanotski Strait; Zimmermann and Prescott, 2021b), and Shelikof Strait (Zimmermann et al., 2019b) points. Bering Strait eastern channel data are included in the plot to show that their cross-sectional areas (overall minimum and minimum through the moorings) exceed the 95 % confidence intervals and are, therefore, more uniformly deeper than expected for their maximum depths.

2.7. Seward Peninsula land features

We utilized additional land features of the Seward Peninsula to aid us in understanding some of the newly described seafloor features. The georegistered, seamless U.S. Geological Survey (USGS) topographic map service (Scale of 1:63,360 for Alaska; https://goto.arcgisonline.com/maps/USA_Topo_Maps), available through ESRI, was used for hand-digitizing the major Seward Peninsula watersheds (Imuruk Basin inside of Grantley Harbor, Tuksuk Channel, and Port Clarence; Golovnin Lagoon within Golovnin Bay; and Norton Bay) along the north shore of Norton Sound. We digitized watershed boundaries by interpreting topographic features such as elevation contours, streams, and ridgelines. We also digitized the Seward Peninsula portion of the Continental Divide of the Americas, which separates watersheds draining into Kotzebue and Norton sounds, and plotted the spatial extent of paleoglaciers from Kaufman and Manley (2004) (https://instaar.colorado.edu/QGISL/ak_paleoglacier_atlas/) in the Seward Peninsula area.

3. Results

3.1. Bathymetry compilation

Our 100 m horizontal resolution bathymetry of the eastern channel of Bering Strait extends across $2500~\rm km^2$, and its depths range from MHW to a maximum of $63.3~\rm m$ (north of the region shown in Fig. 3). This new bathymetry shows that the Cape Prince of Wales Shoal branches off from the coastal inshore area at a depth of $\sim 7.5~\rm m$, just north of the narrowest part of the eastern channel, producing an underwater barrier to the flow of deeper waters. The shoal rises as much as $5~\rm m$ above the deeper and relatively flat area between it and the mainland. The seaward side of the shoal is steep, especially near the cape, rapidly dropping off from 10 to 40 m in depth in $<2~\rm km$. Broad shoals extend from the northwest and southwest coasts of Little Diomede Island. Narrow shoals curve northward from the southeastern tip of Little Diomede Island, and northward and southward from Fairway Rock.

3.2. Minimal openings

The smallest opening of the eastern channel of the strait starts about 8 km north of Wales, zigzags in a WNW direction for a curved distance of 40.1 km (37.0 km straight length), reaches a maximum depth of 54.2 m near the center of the channel, and ends on the southeast corner of Little Diomede Island (Fig. 3). This minimal cross-section of 1.8 km² occurs about 5 to 10 km south of the APL moorings (Table 2). Across the moorings, the minimal cross-sectional opening starts about 9 km north of Wales, ends at the northeast corner of Little Diomede Island, is 2.0 km² in area, 44 km in curved length (38.7 km straight length), and has a maximum depth of 59.3 m. Because of the need to accommodate multiple waypoints along its path, the tortuosity of the moorings cross-section (1.14) is higher than the minimal cross-section (1.08). Although it is located in a shallow part of the eastern strait, Fairway Rock is too far south to be included in a minimal opening.

We plotted the cross-sectional area and maximum depth of these eastern channel cross-sections to compare them to measurements of other recently derived Alaska inlets (Fig. 4). We found that with both

Table 2Minimal cross-sectional openings of the Eastern Channel of the Bering Strait.
Tortuosity is the curved length divided by the straight length.

Cross- sections	Area (km²)	Maximum depth (m)	Curved length (km)	Straight length (km)	Tortuosity
Minimal	1.819	54.2	40.1	37.0	1.08
Moorings	1.999	59.3	44.1	38.7	1.14
Pre- erosion	1.779	53.2	40.1	37.0	1.08

variables transformed by LOG₁₀, there exists a significant linear correlation (df = 43, F = 303, P < 0.001, R^2 = 0.88) between pass cross-sectional area and maximum depth,

$$Log_{10}(Area) = 1.9 \times Log_{10}(Depth) + 1.9,$$

where $Log_{10}(Area) = LOG_{10}$ of minimal cross-sectional area in meters squared (m²); and.

 $\mbox{Log}_{10}(\mbox{Depth}) = \mbox{LOG}_{10}$ of the maximum depth of the minimal cross-section in meters.

Our two estimates of cross-sectional area for the Bering Strait - not included in the regression - are relatively large for their maximum depths, exceeding the 95 % confidence intervals. This implies that the strait is more uniformly deep than typical for inlets with this same maximum depth.

3.3. Depth change

The overlap between the ~ 2010 multibeam raster of 4 m horizontal resolution and the ~ 1950 smooth sheet soundings is limited to an area of $\sim 560~\text{km}^2$ within the eastern portion of the eastern channel. Depth differences show that much of this overlap has experienced erosion, some of it > 1 m (Fig. 5). The Cape Prince of Wales Shoal has also eroded by > 1 m along 16 km of its seaward face, effectively widening the northern entrance to the strait. The only exceptions to this general erosion were deposition > 1 m in a small, deep area near the center of the strait, deposition < 0.5 m in an area 13 km in length seaward of the Cape Prince of Wales Shoal erosion, and deposition < 0.5 m in a triangular area shoreward of the shoal.

We had no means of testing for the statistical significance of this general > 1 m of erosion within the strait, but deposition of > 1 m over ~ 70 years caused substantial inshore changes in the Chignik area of Alaska (Zimmermann et al., 2018). Similarly, erosion and deposition of > 1 m over ~ 40 to ~ 70 years substantially reshaped portions of Alaska's Beaufort Sea coast (Zimmermann et al., 2022). Therefore, we artificially shallowed our Bering Strait depth surface by 1 m and reran the minimal cross-section process to determine how much change there might have been due to widespread erosion over ~ 60 years. We found that the theoretical pre-erosion strait (1.779 km²; Table 2) had decreased only a small amount (~ 2 %) over the original estimate (1.819 km²), both still rounding to 1.8 km².

3.4. Seafloor features

While our 100 m horizontal resolution raster helps clarify the previously known Cape Prince of Wales Shoal and other shoals, it also shows several previously undescribed features in the eastern channel (Fig. 3). A shore-parallel bar is apparent along the NW face of Cape Prince of Wales Spit (Short, 1975). Offshore sediment waves, seafloor gouges, and a broad seafloor channel are also apparent in the 100 m bathymetry, but often clearer in the 4 m multibeam bathymetry.

(i) Offshore bar

The bar occurring off of Cape Prince of Wales Spit is about 300–400 m wide, about 1 m tall, within ~ 1 km of the spit (Fig. 6A), and visible along about 17 km of shoreline (Fig. 3). This seafloor feature is distinct enough to be depicted clearly in the 1950 smooth sheet data of survey H07845 (all of the other features occur in the area covered by multibeam surveys). This bar appears similar in morphology to the alternating patterns of light and dark areas of Cape Prince of Wales Spit, presumably showing a history of shoreline accretion. Short (1975) described three types of these offshore bar features as occurring along the Alaska coast of the Chukchi and Beaufort seas.

(ii) Sediment waves

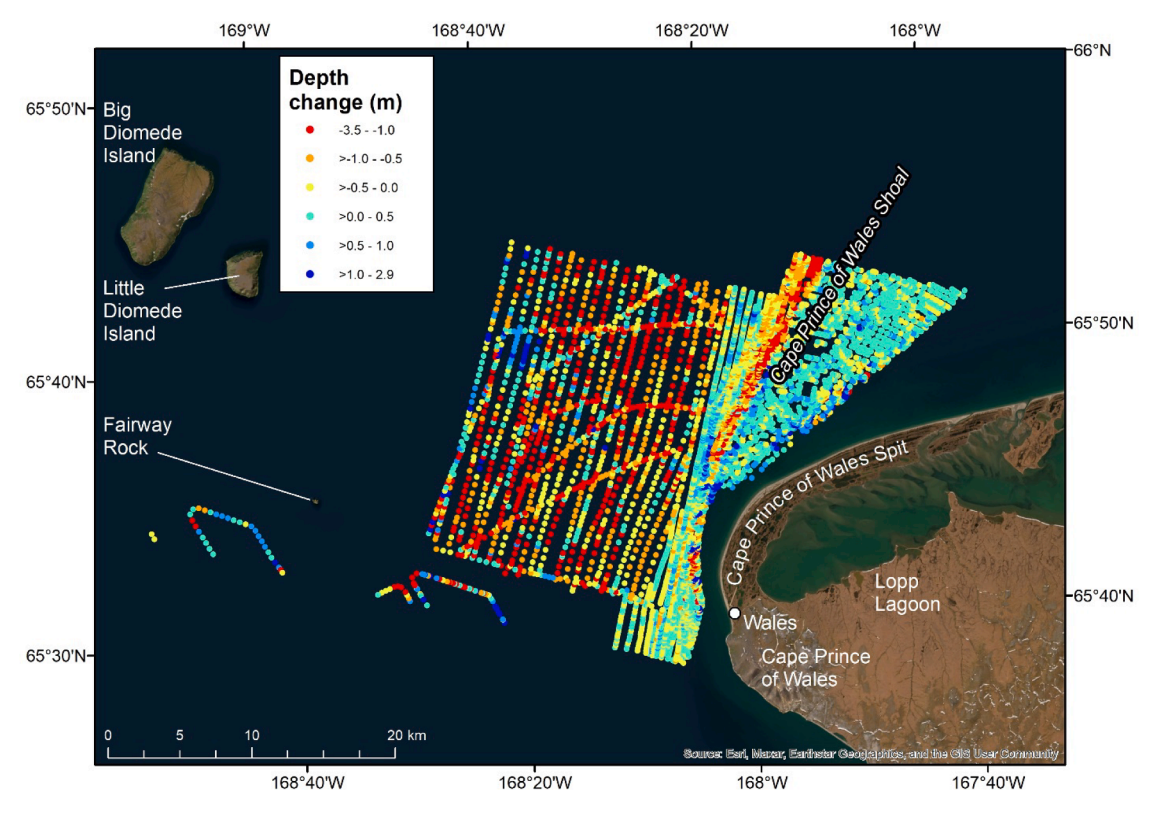


Fig. 5. Depth differences (\sim 1950 minus \sim 2010) between the original (\sim 1950) smooth sheet soundings and depths from the composite 4 m horizontal resolution multibeam raster (\sim 2010). Hot colors indicate erosion and cold colors indicate deposition.

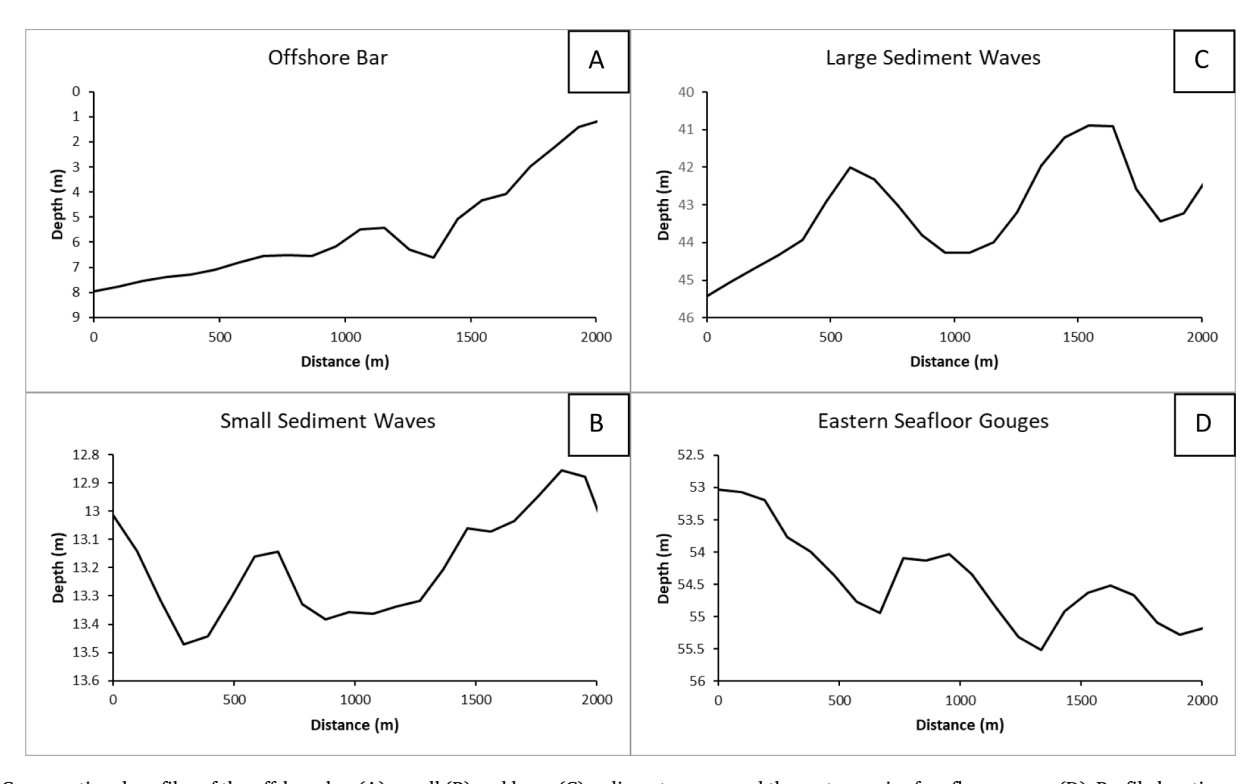


Fig. 6. Cross-sectional profiles of the offshore bar (A), small (B) and large (C) sediment waves, and the eastern pair of seafloor gouges (D). Profile locations are shown in Fig. 3.

Small sediment waves measuring ~ 0.5 to ~ 1.0 m high from crest to trough with the crests oriented perpendicular to the coast occur in an area about 3 to 6 km offshore of the Cape Prince of Wales Spit (Fig. 3;

Fig. 6B). There are larger sediment waves seaward of Cape Prince of Wales Shoal, measuring ~ 2 m tall, with crests oriented on a roughly north–south axis and parallel to the shoal (Fig. 6C). Both sets of sediment

waves are ~ 1 km from crest to crest. Surficial sediment samples of silt occur near the small waves. Stones, along with a "No Sample Obtained," indicate hard bottom near the large waves. The lowest multibeam backscatter of the strait, presumably indicating softer sediments, occurs just landward of the large sediment waves (Fig. 7).

(iii) Seafloor gouges

Two pairs of short (\sim 2 km long), roughly parallel, 2 m deep gouges in the seafloor occur in the area north and west of APL mooring A2-10, with a western pair extending NW/SE and an eastern pair extending NE/SW (Fig. 6D), reaching to the northern edge of the bathymetry (Fig. 3). South of these 200 m wide gouges, the seafloor is flatter, the seafloor features are fainter, and much more visible in the 4 m than the 100 m resolution raster. In the area between moorings A2-10 and A2W-10 and extending south to the minimal cross-section, there are numerous small (\sim 0.5 m) elevations and depressions without any discernable pattern. A single sediment sample in this area contained stones, and the backscatter indicates hard seafloor but no differences between peaks and troughs of these features (Fig. 7). We suspect that even though these two pairs of seafloor gouges occur between about 51 to 55 m in depth, they may be from historic or recent ice keels.

(iv) Seafloor Channels

Near the north and center of the eastern channel, and in its deepest part, is a nearly linear seafloor channel, $\sim\!\!1$ to 2 km wide, oriented along a roughly N/S axis. This feature is generally bounded by the 55 m depth contour and is $\sim\!4$ m deeper than the surrounding seafloor (Fig. 3) along its $\sim\!75$ km length (outlined in white in Fig. 8), extending far into the Chukchi Sea. Just to the south of the minimal cross-section across the

APL moorings, this seafloor channel appears to divide into a broad and a narrow branch. The broad branch extends toward the southern end of Lopp Lagoon but stops about 8 km west of it. The narrow branch extends southward, toward the North Eastern Bering Sea, and divides into two paths around a shoal before continuing to the southern edge of the bathymetry raster. The seafloor channel area, including its broad and narrow branches, appears as hard seafloor in the multibeam backscatter. The sediment samples primarily consist of stone, with some pebbles, broken shells, and mud (Fig. 7).

(v) Potential Paleodrainages

Plotting the strait with the neighboring North Eastern Bering Sea Slope (Zimmermann and Prescott, 2018) and Norton Sound (Prescott and Zimmermann, 2015) bathymetry rasters shows three Norton Sound features that might be paleodrainages (Bond, 2019; J. C. Hill, U.S. Geological Survey, pers. comm., May 4, 2021) - relic, late glacial seafloor channels or canyons formed by the erosive force of runoff from rapidly melting glaciers (Fig. 8). These potential paleodrainages originate from western, central, and eastern Norton Sound and extend northwestward toward the eastern channel of Bering Strait. These potential paleodrainage features are similar to those found nearby in the Chukchi Sea through sub-bottom profiling (Hill et al., 2007; Hill and Driscoll, 2008; Stockmaster, 2017) but with some significant differences. The Norton Sound features are mostly not filled in with sediment, visible in the bathymetry surface, occur nearshore, and mostly parallel the coastline. The Chukchi features are completely filled in with sediment, not visible in the unknown bathymetry utilized by Hill et al. (2007), Hill and Driscoll (2008), and Stockmaster (2017), occur far off of the present shoreline and are mostly perpendicular to the coastline. Hope Valley, located within Kotzebue Sound, may be the eastern end of

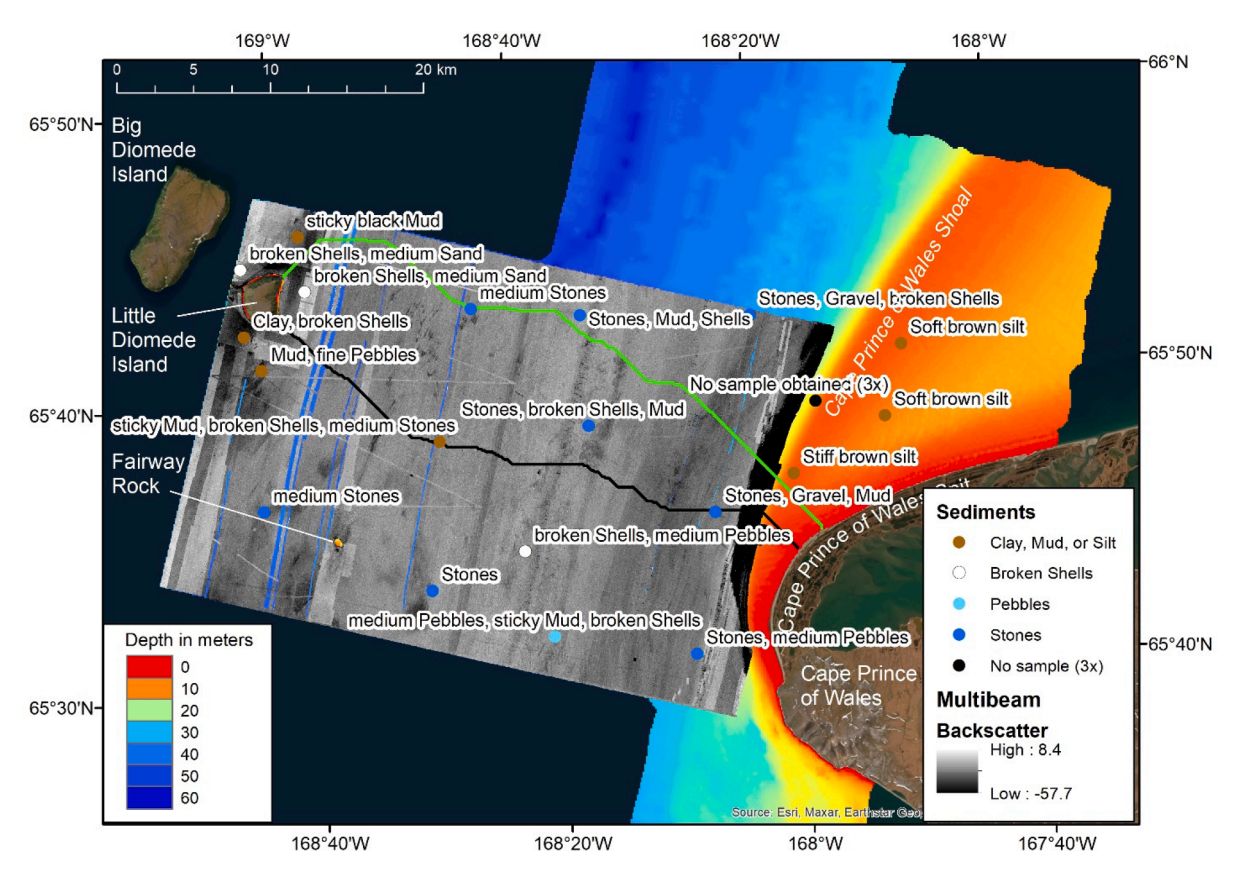


Fig. 7. Multibeam backscatter plotted on top of bathymetry. Note that colors from the bathymetry show through where there are north/south oriented gaps in the composite backscatter image. Sediment samples collected during the multibeam surveys are also shown. One sediment sample was reported as "No sample obtained" three times in a row, probably indicating hard bottom that the sediment sampler could not penetrate.

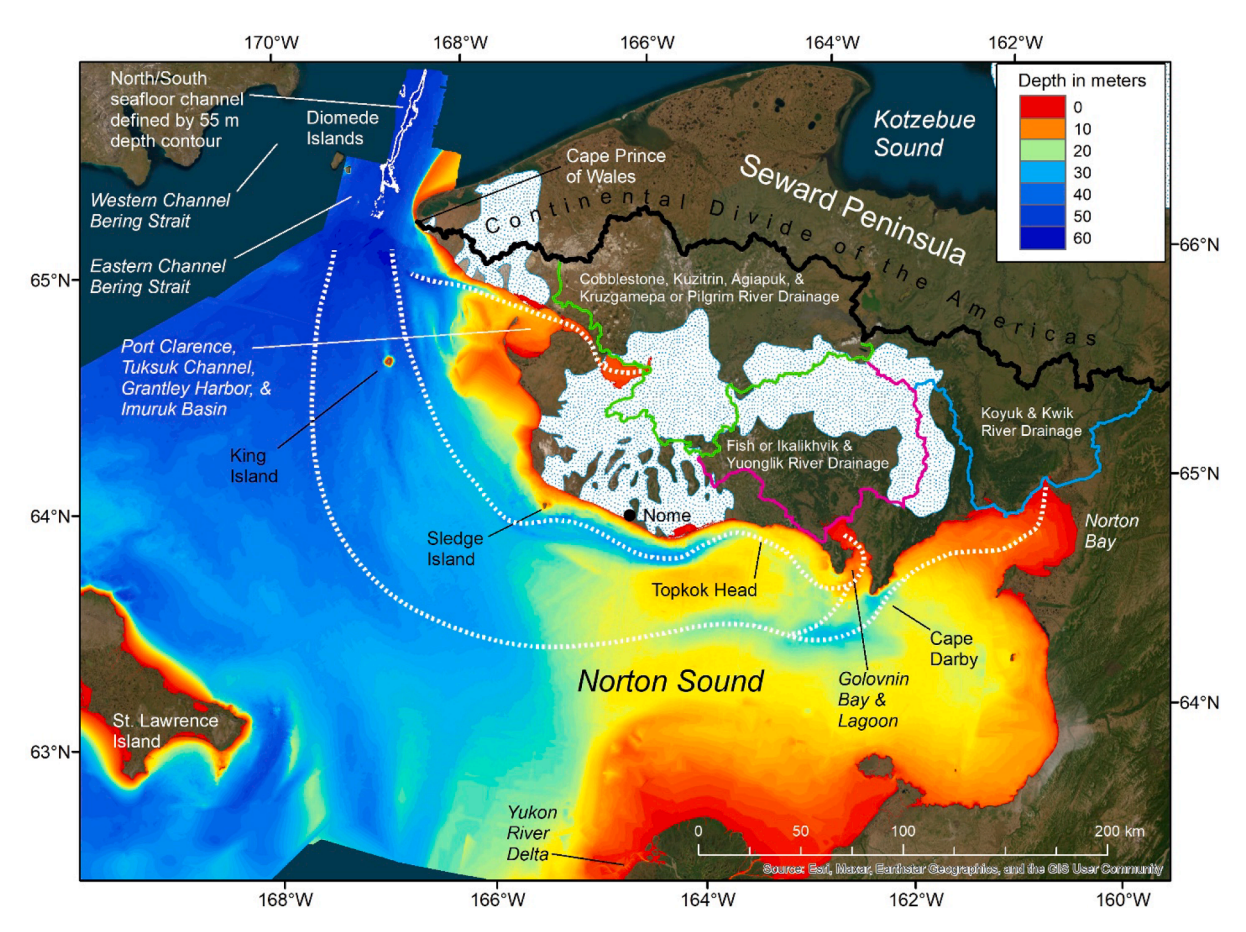


Fig. 8. Combined bathymetry rasters of the eastern channel of the Bering Strait, North Eastern Bering Sea Slope (Zimmermann and Prescott, 2018), and Norton Sound (Prescott and Zimmermann, 2015). Portions of tidal channels or potential paleodrainages are visible in the Norton Sound bathymetry. Dashed white lines indicate what we hypothesize to be their full length, extending eastward to outlets of the three large drainages on the north shore of Norton Sound and extending westward towards the seafloor channel bounded by the 55 m depth contour in the eastern channel of the Bering Strait. Drainages and the Continental Divide of the Americas were digitized from the seamless U.S. Geological Survey (USGS) topographic map service (Scale of 1:63,360 for Alaska; http://goto.arcgisonline.com/maps/USA_Topo_Maps), available through ESRI. Paleoglaciers from Kaufman and Manley (2004; http://instaar.colorado.edu/QGISL/ak_paleoglacier_atlas/) are represented as white areas stippled with blue on the Seward Peninsula.

another paleodrainage, isolated from other similar offshore features due to sediment deposits obscuring its westward end (Keigwin et al., 2006).

The westernmost potential paleodrainage is the shortest (\sim 25 km) and shallowest (only \sim 3 m deeper than the offshore seafloor). Its east end points directly into Port Clarence, which is connected to Grantley Harbor, Tuksuk Channel, and Imuruk Basin (Fig. 8). Seward Peninsula watersheds draining into Port Clarence collectively cover only about 800 km² of land and therefore seem unlikely to be a source of runoff for creating this potential paleodrainage. Our analysis of the USGS topography determined that the Cobblestone, Kuzitrin, Agiapuk, and the Kruzgamepa or Pilgrim rivers drain a much larger watershed (10,050 km²) into Imuruk Basin, making it seem a more likely origin for the potential paleodrainage. The Imuruk Basin watershed extends to the Continental Divide and overlaps with a substantial amount of paleoglacier (Kaufman and Manley, 2004).

The central potential paleodrainage runs roughly parallel and near the north shore of Norton Sound, is about 15–20 km wide, and about 5 to 10 m deeper than the offshore area just seaward of Sledge Island (Fig. 8). Offshore of Nome it narrows to about 13 km, deepens to about 20 m deeper than the offshore area, gets closer to the mainland, and near Topkok Head, it appears to end in an area near only small mainland drainages. Between the eastern end of this paleodrainage and the entrance to Golovnin Lagoon and Bay, there are isolated deeper areas along with some shallower features arcing into Golovnin Bay. We interpret this area of uneven bathymetry to be partial sedimentation of the eastern or northeastern end of this potential paleodrainage which we

hypothesize originated within Golovnin Bay and Lagoon. The larger Fish or Ikalikhvik River, along with the smaller Yuonglik River to the east, drain a basin that is 6140 km² and empty into the head of Golovnin Lagoon. The Golovnin watershed also overlaps with a substantial amount of paleoglacier (Kaufman and Manley, 2004) but it does not quite reach the Continental Divide.

The easternmost potential paleodrainage is somewhat similar in size and shape as the central one, but it is interrupted by shoals and much less apparent as a channel- or canyon-like feature (Fig. 8). From its deepest point directly south of Golovnin Bay, where it is about 20 m deeper than the offshore area, this potential paleodrainage heads northeast toward Cape Darby at the outer edge of Norton Bay. At Cape Darby, it follows the shore for about 15 km towards Norton Bay but then appears to end about 90 km away from the eastern shore of Norton Bay and the terminus of the large Koyuk River. The Koyuk, along with the much smaller Kwik River, drain a basin of 5800 km² into the head of Norton Bay, which we hypothesize is the likely origin of this eastern potential paleodrainage. The Norton Bay watershed extends to the Continental Divide but overlaps with only a minor portion of paleoglacier (Kaufman and Manley, 2004).

We could find no similar potential paleodrainages near the branch of the eastern strait seafloor channel that extended southeasterly toward Lopp Lagoon. Examination of the topography in this area showed that there are numerous small watersheds, each about 5 to 15 km in length, entering the south side of Lopp Lagoon. The largest watershed, entering the east end of Lopp Lagoon, is that of the Mint River (500 km 2), but this

is much smaller than the potential paleodrainage-associated watersheds along the north shore of Norton Sound. North of the Mint River, the rivers drain into a different lagoon. All of these watersheds occur north of the Continental Divide.

4. Discussion

We created a seamless, detailed bathymetric map of the Bering Strait's eastern channel from partially overlapping data sets of two eras (~1950, ~2010), using similar methods as for several previously published regional bathymetric maps of Alaska. This shore-to-shore bathymetry enabled the first formal derivation of the position and size of the eastern channel's minimal opening and size estimate of a second opening across the flux measurement moorings - two important oceanographic reference points. While these two cross-sectional openings were 10 % and 20 % larger, respectively, than previously estimated, they were within the level of uncertainty previously stated (Woodgate et al., 2005), and these new assessments of larger eastern channel sizes are dwarfed by the seasonal and annual variability in flux. The impact of our new cross-sectional estimates will be known only when they are incorporated into oceanographic models of sufficient horizontal resolution (~1 km). Overlapping bathymetry from the two eras showed that there has been extensive erosion > 1 m, potentially facilitating greater northward flow of Bering and ACC waters, but the eastern channel was already relatively deep for its size, and the impact of this erosion on total cross-sectional area was minimal (~2 %). This new bathymetry was detailed enough to clearly depict several previously undescribed seafloor features and, while we can hypothesize on their origins and what they mean for previous and future depth changes in the strait, more geological information is needed for definitive analyses.

4.1. Sources of errors

(i) Bathymetry

Questions always arise about the quality of older bathymetry data sets and the utility of making comparisons to more recent bathymetry data collected with superior technology (e.g., navigation, speed of sound corrections, echosounding, and computerized data collection). We have shown that with careful proofing and editing, it is at least possible to fix georeferencing and digitization errors so common in these NCEI smooth sheet data (Zimmermann and Benson, 2013). Once these edits are implemented, smooth sheet data collected since 1930 are quite comparable to recent data (Zimmermann et al., 2019a). All data utilized in this project were from 1950 or later, and occurred close to land, facilitating the use of nearby visual or radio navigational stations (Table 1). Using similar methods, analyses have successfully quantified depth change over several decades, providing insight on coastal erosion and deposition processes (Zimmermann et al., 2018; Zimmermann et al., 2022).

(ii) Tide/Sea level measurements

Hydrographers corrected for tides, according to standard protocols, both the ~ 1950 and ~ 2010 bathymetry data sets we utilized in this analysis. Unfortunately, placement of tide stations inside of Lopp Lagoon during the ~ 1950 surveys, and reliance on the CO-OPS Red Dog Dock station near Kotzebue during the ~ 2010 surveys, may have provided corrections more appropriate for areas north of the strait. This may be a significant source of error for soundings collected within the strait, as this inlet is so constricted that Pacific and Arctic Ocean waters have different elevations, with the Pacific waters generally 0.5 m higher in elevation than the Arctic waters (Stigebrandt, 1984; Overland and Roach, 1987). However, this situation is highly variable as winds can increase this elevation difference, or reverse it, such that Arctic waters flow into the Pacific (Coachman and Aagaard, 1988). For example, the DR for

multibeam survey H12228 noted that winds up to 25 knots blew almost constantly from the north or south (https://data.ngdc.noaa.gov/platforms/ocean/nos/coast/H12001-H14000/H12228/DR/H12228.pdf), indicating that multiple reversals may have occurred during that survey. While we could detect minor artifacts in the bathymetry from crossline checks, which were also highly visible in the multibeam backscatter (Fig. 7), any impact of sea level change was not detected in the multibeam data. Our finding of relatively homogenous areas of erosion and deposition also indicated minimal impacts from tide or sea level measurement errors.

4.2. Other Bering Strait size estimates:

(i) Estimates in oceanographic models

Oceanographers and oceanographic modelers have previously created rough size estimates of the total Bering Strait. To do this, they have mostly used published bathymetry compilations or navigational charts rather than the hydrographic smooth sheets and multibeam surveys that we used in this analysis, probably due to the availability of the published compilations and the difficulty in working with raw soundings. It is important to recognize that the grid spacing on these models allows only a few points across the strait, and the sections presented often do not align with what would be the narrowest crossing.

Clement Kinney (2014) helpfully summarized strait size estimates for five of these oceanographic models, with the largest estimate roughly double that of the smallest estimate, perhaps due to differences in their underlying bathymetry sources, differences in horizontal resolution, or the need to modify the bathymetric surface to facilitate the functionality of each model. The largest strait estimate of 4.50 km² was from ECCO2 model's (Menemenlis et al., 2008) blend of Smith and Sandwell (1997) and the General Bathymetric Chart of the Oceans (GEBCO: htt ps://www.gebco.net/) data at a resolution of ~ 23 km. The next largest strait estimate of 4.17 km² was from the ORCA (Brodeau et al., 2010) model that utilized ETOPO2 (https://www.ngdc.noaa.gov/mgg /global/etopo2.html) bathymetry at a \sim 13 km resolution. The middle-sized strait estimate of 3.24 km² came from the BESTMAS model (Zhang et al., 2010), derived at a horizontal resolution of ~ 4 km from a mixture of IBCAO (International Bathymetric Chart of the Arctic Ocean; Jakobsson et al., 2000) and ETOPO5 (Earth Topography Five Minute Gridded Elevation Data; https://www.ngdc.noaa.gov/mgg/global/eto po5.HTML) data (Holland, 2000). The smallest strait estimates were from the PIOMAS (Zhang et al., 2008) model (2.38 km²), which is a coarser version (~40 km resolution) of the BESTMAS model, and from the NAME (Maslowski et al., 2004) model (2.37 km²) using ETOPO5 bathymetry, with a resolution of ~ 9 km.

Only the NAME (Maslowski et al., 2004) and BESTMAS (Zhang et al., 2010) models were of high enough resolution to resolve the strait into western and eastern channels, but BESTMAS was the only one that separated the channels by land (see Figure 7.2 in Clement Kinney et al., 2014). Separate channel size estimates were not published, thus making comparisons to our eastern channel size estimate problematic. If we utilize additional information from Woodgate et al.'s (2005) estimates, where their western channel is 1.0 km 2 or 38.5 % of the total strait and their eastern channel is 1.6 km 2 or 61.5 % of the total strait, then the eastern channel for ECCO2 (2.8 km 2), ORCA (2.6 km 2), and BESTMAS (2.0 km 2) model estimates are larger, and the PIOMAS (1.5 km 2) and NAME (1.5 km 2) model estimates are smaller than our estimate.

(ii) Estimates derived from bathymetry

A few oceanographic researchers have derived strait size estimates from raw bathymetry and distance estimates. Using the same eastern channel to strait ratio from Woodgate et al. (2005), Dall's (1882) total strait estimate of 3.9 km² converts to 2.4 km², Overland and Roach's (1987) total strait estimate of 4.1 km² converts to 2.5 km², and Coachman and

Aagaard's (1981) total strait estimate of 4.25 km² converts to 2.6 km². While all of these are much larger than our estimate, they are arguably more comparable to our work than the model estimates.

4.3. Possible causes of erosion:

(i) UNAVCO land rise

Apparent depth changes that we observed in our analyses may have been influenced by changes in land level over time. The nearest UNAVCO (University Navigation Signal Timing and Ranging Consortium) station (AB09; https://www.unavco.org/instrumentation/networks/status/nota/overview/AB09), which measures horizontal and vertical land movement by recording GPS (Global Positioning System) positions, is located inland of Wales. Since AB09's installation date of July 2007, the station has been relatively stationary. It has only been moving south at an average rate of 2.51 mm yr $^{-1}$, east 2.65 mm yr $^{-1}$, and down 0.90 mm yr $^{-1}$. Thus, over our \sim 60 year time frame, the land has shifted about 54 mm or 0.054 m downward, in the direction that would add to our finding of erosion, but a negligible amount compared to our \pm 1 m depth changes over the same time frame.

(ii) CO-OPS sea level change

Depth changes that we observed in our analyses may also have been influenced by long-term sea level changes over time. The nearest NOAA CO-OPS (Center for Operational Oceanographic Products and Services) tide stations are 190 km to the southeast of the strait at Nome (accessed August 2, 2022; https://tidesandcurrents.noaa.gov/stationhome.html? idhttps://tidesandcurrents.noaa.gov/stationhome.html?id=9468756) and 290 km to the northeast of the strait at Red Dog Dock (accessed August 2, 2022; https://tidesandcurrents.noaa.gov/stationhome.html? id=9491094). Relative sea level is increasing at the Nome tide station at a rate of 3.89 mm yr⁻¹ since 1992, but this information is not available for the Red Dog Dock station. Over the roughly 60-year time period of our depth comparison, relative sea level may have increased about 233.4 mm or 0.2 m, making the water in the strait area deeper. This relative sea level change is again far below the $\pm~1$ m depth differences we quantified, but would have acted to increase the amount of apparent deepening from erosion.

(iii) Currents

The much-studied Bering Strait currents are an obvious potential source of sediment erosion. Unfortunately, the common sediment classification of "stones" within the strait is not one of the designated size categories in Wentworth's (1922) widely used scale, but since the hydrographers also used the grain size term of pebbles (2 to 64 mm), we assume that the term of stones is equivalent to cobbles, which are 64 to 256 mm in diameter. Woodgate (2018) shows near-bottom annual mean currents up to about 35 cm/s near the middle of the east channel of the strait at mooring A2 (and the mode of hourly currents rising from ~ 30 cm/s in the 1990 s to 2000 s to \sim 50 cm/s in 2014–2015, Woodgate, UW, APL, pers. comm.), so friction from the movement of water to the point of critical shear stress for these stones or cobbles is an obvious potential cause of erosion (Fischenich, 2001). Drop camera observations show that much of the strait is bare rock with loose rock and gravel nearer to Cape Prince of Wales (Fig. 3 of Cooper et al., 2019; L. W. Cooper, University of Maryland Center for Environmental Science, pers. comm., April 25, 2023).

Woodgate et al. (2015) show in satellite imagery (see their Fig. 1A) a vast sediment plume within the ACC, stretching roughly 200 km from the strait to the seaward edge of Kotzebue Sound. This plume appears to originate north of Cape Prince of Wales and landward of its shoal, in an area with silty sediment, which, if it is unconsolidated, should be easily mobilized by light currents (<0.035 ft/sec or 1.1 cm/sec) (Fischenich,

2001). While this seems like a plausible origin, this silty area showed light deposition in our analysis, so we hypothesize that another likely origin of the plume is the eroding seaward side of the shoal.

(iv) Ice

Despite much of the strait being deeper than 50 m, ice is another possible agent of sediment erosion. Roach et al. (1995) mentioned that Bering Strait oceanographic instruments could not be placed within about 40 m of the surface due to deep-keeled ice floes. Woodgate et al. (2016) report instrument damage consistent with impacts from ice floes at about 45 m during the winter of 2015/2016. Indigenous knowledge reports icebergs or thick multiyear ice coming south through the strait within the oral record (Raymond-Yaboubian et al., 2014), and even in modern times (winter 2011-2012) satellites have tracked multiyear ice south through the strait from the Beaufort Sea (Babb et al., 2013). While ridging or iceberg draft to these water depths has not been directly observed, there has been recent (winter 2015-2016) damage to mooring instrumentation at \sim 45 m depth which is most likely attributable to ice (Woodgate et al., 2016). A study of satellite data from 1974 to 1985 showed formation of double ice arches in the strait, a compression feature that presumably also led to significant ice ridging (Torgerson and Stringer, 1985). It has been hypothesized (De Boer and Nof, 2004, a and b) that roughly 11,000 years before present (the start of the Holocene), the Bering Strait opened abruptly due to the breakup of an ice dam. However, ice is unlikely to give a strait-wide deepening.

5. Conclusions

We thus conclude that the most likely cause of seafloor erosion is increasing currents (Woodgate, 2018) in the strait. We suspect that ice floe keels may also have contributed to the erosion from time to time, but the currents are the most likely explanation for why the strait is largely swept clean of smaller grain sizes, except in depressions and protected areas. The areas of sediment waves near Cape Prince of Wales Spit and Shoal also support this idea. Land subsidence and sea level rise only made small contributions to the apparent erosion. Current-driven erosion has made this small strait deeper than expected. Seafloor features with paleodrainage-like similarities suggest that it was Seward Peninsula paleoglacier freshwater runoff, and not seawater, that first led to a temporary reopening of the strait, creating the seafloor channel within the strait's deepest locations. We also conclude that the depth change over time has not caused the increasing currents; however, increasing currents and increasing strait size may form a positive feedback loop, exacerbating an established trend of greater northward throughflow in recent decades with significant climate change implications (Woodgate, 2018).

Declaration of Competing Interest

The authors declare that they have no known competing financial interests or personal relationships that could have appeared to influence the work reported in this paper.

Data availability

Data will be made available on request.

Acknowledgments

Thank you to Jenna Hill, USGS, Santa Cruz, California, USA and Patrick Lajeunesse, Department of Geography, Université Laval, Canada, for geological advice. Thank you to Todd TenBrink, Jaclyn Clement Kinney, Ned Laman and Michael Martin for helpful manuscript reviews. We thank Lee Cooper and an anonymous reviewer at Progress in Oceanography. Thanks to the staff at NCEI (National Centers for

Environmental Information: http://www.ngdc.noaa.gov) for frequent assistance with bathymetry data. The findings and conclusions in the paper are those of the author(s) and do not necessarily represent the views of the National Marine Fisheries Service. Any use of trade, product, or firm names in this publication is for descriptive purposes only and does not imply endorsement by the U.S. Government.

References

- Aagaard, K., Carmack, E.C., 1989. The role of sea ice and other fresh water in the Arctic circulation. J. Geophys. Res. Oceans 94 (C10), 14485–14498.
- Babb, D.G., Galley, R.J., Asplin, M.G., Lukovich, J.V., Barber, D.G., 2013. Multiyear sea ice export through the Bering Strait during winter 2011–2012. J. Geophys. Res. Oceans 118 (10), 5489–5503. https://doi.org/10.1002/jgrc.20383.
- Bloom, G.L., 1964. Water transport and temperature measurements in the eastern Bering Strait, 1953–1958. J. Geophys. Res. 69 (16), 3335–3354.
- Bond, J.D., 2019. Paleodrainage map of Beringia. Yukon Geological Survey, Open File 2019-2
- Brodeau, L., Barnier, B., Treguier, A.M., Penduff, T., Gulev, S., 2010. An ERA40-based atmospheric forcing for global ocean circulation models. Ocean Model 31 (3–4), 88–104. https://doi.org/10.1016/j.ocemod.2009.10.005.
- Clement Kinney, J., Maslowski, W., Aksenov, Y., de Cuevas, B., Jakacki, J., Nguyen, A.n., Osinski, R., Steele, M., Woodgate, R.A., Zhang, J., 2014. On the Flow Through Bering Strait: A Synthesis of Model Results and Observations. In: Grebmeier, J.M., Maslowski, W. (Eds.), The Pacific Arctic Region: Ecosystem Status and Trends in a Rapidly Changing Environment. Springer Netherlands, Dordrecht, pp. 167–198.
- Coachman, L.K., Aagaard, K., 1981. Re-evaluation of water transports in the vicinity of Bering Strait. In: Hood, D.W., Calder, J.A. (Eds.), The Eastern Bering Sea Shelf: Oceanography and Resources. National Oceanic and Atmospheric Administration, Washington, D.C., pp. 95–110
- Coachman, L.K., Aagaard, K., 1988. Transports through Bering Strait: Annual and interannual variability. J. Geophys. Res. Oceans 93 (C12), 15535–15539.
- Cooper, L.W., Guarinello, M.L., Grebmeier, J.M., Bayard, A., Lovvorn, J.R., North, C.A., Kolts, J.M., 2019. A video seafloor survey of epibenthic communities in the Pacific Arctic including Distributed Biological Observatory stations in the northern Bering and Chukchi seas. Deep Sea Res. Part II 162, 164–179.
- Dall, W.H., 1882. Report on the currents and temperatures of Bering Sea and the adjacent waters. Appendix 16-1880, p. 297-340. U.S.- C.G.S., Rept. Superintendent for the fiscal year ending with June, 1880. Government Printing Office.
- de Boer, A.M., Nof, D., 2004a. The exhaust valve of the North Atlantic. J. Climate 17 (3), 417–422. https://doi.org/10.1175/1520-0442.
- De Boer, A.M., Nof, D., 2004b. The Bering Strait's grip on the northern hemisphere climate. Deep Sea Res. Part I 51 (10), 1347–1366. https://doi.org/10.1016/j.dsr.2004.05.003.
- Erlandson, J.M., Graham, M.H., Bourque, B.J., Corbett, D., Estes, J.A., Steneck, R.S., 2007. The kelp highway hypothesis: marine ecology, the coastal migration theory, and the peopling of the Americas. J. Island Coastal Archaeol. 2 (2), 161–174.
- Fischenich, J.C., 2001. Stability thresholds for stream restoration materials. USAE Research and Development Center, Environmental Laboratory, 3909 Halls Ferry Rd., Vicksburg MS 39180.
- Hayes, D., 2001. Historical atlas of the North Pacific Ocean: maps of discovery and scientific exploration, 1500–2000. Sasquatch Books.
- Hill, J.C., Driscoll, N.W., Brigham-Grette, J., Donnelly, J.P., Gayes, P.T., Keigwin, L., 2007. New evidence for high discharge to the Chukchi shelf since the Last Glacial Maximum. Quat. Res. 68 (2), 271–279.
- Hill, J.C., Driscoll, N.W., 2008. Paleodrainage on the Chukchi shelf reveals sea level history and meltwater discharge. Mar. Geol. 254 (3–4), 129–151.
- Holland, D.M., 2000. Merged IBCAO/ETOPO5 global topographic data product. National Geophysical Data Center (NGDC), Boulder Colorado.
- Hopkins, D.M., ed. 1967. The Bering land bridge (Vol. 3). Stanford University Press, Redwood City, A, USA, xiii \pm 495 pp.
- Hopkins, D.M., Matthews, J.V. and Schweger, C.E. eds., 1982. Paleoecology of Beringia. Wenner-Gren Foundation for Anthropological Research, Symposium 81, Burg Wartenstein, Austria, June 8-17, 1979, Academic Press, New York, xiv + 489 pp.
- Hultén, E., 1937. Outline of the history of arctic and boreal biota during the Quaternary Period: their evolution during and after the glacial period as indicated by the equiformal progressive areas of present plant species. Bokförlags aktiebolaget Thule, Stockholm.
- Jakobsson, M., Cherkis, N., Woodward, J., Macnab, R., Coakley, B., 2000. New grid of Arctic bathymetry aids scientists and mapmakers. Eos Trans. AGU 81 (9), 89–96.
- Jakobsson, M., Pearce, C., Cronin, T.M., Backman, J., Anderson, L.G., Barrientos, N., Björk, G., Coxall, H., de Boer, A., Mayer, L.A., Mörth, C.M., 2017. Post-glacial flooding of the Bering Land Bridge dated to 11 cal ka BP based on new geophysical and sediment records. Clim. Past 13 (8), 991–1005.
- Kaufman, D.S. and Manley, W.F., 2004. Pleistocene maximum and Late Wisconsinan glacier extents across Alaska, USA. In Developments in quaternary sciences (Vol. 2, pp. 9-27). Elsevier.
- Keigwin, L.D., Donnelly, J.P., Cook, M.S., Driscoll, N.W., Brigham-Grette, J., 2006. Rapid sea-level rise and Holocene climate in the Chukchi Sea. Geology 34 (10), 861–864.
- Kumar, A., Yadav, J., Mohan, R., 2020. Global warming leading to alarming recession of the Arctic sea-ice cover: insights from remote sensing observations and model reanalysis. Heliyon 6 (7), e04355.

- Maslowski, W., Marble, D., Walczowski, W., Schauer, U., Clement, J.L., Semtner, A.J., 2004. On climatological mass, heat, and salt transports through the Barents Sea and Fram Strait from a pan- Arctic coupled ice-ocean model simulation. J. Geophys. Res. 109, C03032. https://doi.org/10.1029/2001JC001039.
- Menemenlis, D., Campin, J.M., Heimbach, P., Hill, C., Lee, T., Nguyen, A., Schodlok, M., Zhang, H., 2008. ECCO2: High resolution global ocean and sea ice data synthesis. Mercator Ocean Quarterly Newsletter 31 (October), 13–21.
- Overland, J.E., Roach, A.T., 1987. Northward flow in the Bering and Chukchi Seas. J. Geophys. Res. Oceans 92 (C7), 7097–7105.
- Overland, J., Dunlea, E., Box, J.E., Corell, R., Forsius, M., Kattsov, V., Olsen, M.S., Pawlak, J., Reiersen, L.O., Wang, M., 2019. The urgency of Arctic change. Polar Sci. 21 6-13
- Paquette, R.A., Bourke, R.H., 1974. Observations on the coastal current of Arctic Alaska. J. Mar. Res. 32 (2), 195–207.
- Peltier, W.R., Fairbanks, R.G., 2006. Global glacial ice volume and Last Glacial Maximum duration from an extended Barbados sea level record. Quat. Sci. Rev. 25 (23–24), 3322–3337.
- Pelto, B.M., 2014. Sedimentological, Geochemical and Isotopic Evidence for the Establishment of Modern Circulation through the Bering Strait and Depositional Environment History of the Bering and Chukchi Seas during the Last Deglaciation. University of Massachusetts Amherst. Masters Theses. 134p. https://scholarworks. umass.edu/masters_theses_2/108. https://doi.org/10.7275/5735252.
- Pico, T., Mitrovica, J.X., Mix, A.C., 2020. Sea level fingerprinting of the Bering Strait flooding history detects the source of the Younger Dryas climate event. Sci. Adv. 6 (9).
- Polyak, L., Darby, D.A., Bischof, J.F., Jakobsson, M., 2007. Stratigraphic constraints on late Pleistocene glacial erosion and deglaciation of the Chukchi margin. Arctic Ocean. Quaternary Research 67 (2), 234–245.
- Prescott, M. M., and Zimmermann, M., 2015. Smooth sheet bathymetry of Norton Sound. U.S. Department of Commerce, NOAA Technical Memorandum NMFS-AFSC-298, 23 p.
- Raymond-Yakoubian, J., Y. Khokhlov, and A. Yarzutkina (2014), Indigenous Knowledge and Use of Bering Strait Region Ocean Currents, edited, p. 126, Final report to the National Park Service, Shared Beringian Heritage Program for Cooperative Agreement H99111100026, Kawerak, Inc., Social Science Program: Nome, AK. Available at http://www.kawerak.org/forms/nr/OC%20report%20for%20web.pdf.
- Richter-Menge, J., Druckenmiller, M.L., 2020. The Arctic. In State of the Climate in 2019. In: Diamond, H.J., Schreck, C.J. (Eds.), vol. 101. Bulletin of the American Meteorological Society, pp. 185–S238.
- Roach, A.T., Aagaard, K., Pease, C.H., Salo, S.A., Weingartner, T., Pavlov, V., Kulakov, M., 1995. Direct measurements of transport and water properties through the Bering Strait. J. Geophys. Res. 100, 18443–18457.
- Royer, T.C., Finney, B., 2020. An oceanographic perspective on early human migrations to the Americas. Oceanography 33 (1), 32–41.
- Serreze, M.C., Barrett, A.P., Slater, A.G., Woodgate, R.A., Aagaard, K., Lammers, R.B., Steele, M., Moritz, R., Meredith, M., Lee, C.M., 2006. The large-scale freshwater cycle of the Arctic, J. Geophys. Res. Oceans 111 (C11).
- Short, A.D., 1975. Offshore bars along the Alaskan Arctic coast. J. Geology 82 (2), 209–221.
- Smith, W.H., Sandwell, D.T., 1997. Global sea floor topography from satellite altimetry and ship depth soundings. Science 277 (5334), 1956–1962.
- Smith, L.C., Stephenson, S.R., 2013. New Trans-Arctic shipping routes navigable by midcentury. Proc. Natl. Acad. Sci. 110 (13), E1191–E1195.
- Stigebrandt, A., 1984. The North Pacific: A global-scale estuary. J. Phys. Oceanogr. 14 (2), 464–470.
- Stockmaster, B.A., 2017. Paleodrainage insights into the fluvial and glacial history of the western Chukchi margin, Arctic Alaska (Doctoral dissertation, Coastal Carolina University). Electronic Theses and Dissertations, 49, https://digitalcommons.coastal.edu/etd/49.
- Torgerson, L.J., Stringer, W.J., 1985. Observations of Double Arch Formation in the Bering Strait. Geophys. Res. Lett. 12 (10), 677–680.
- Wentworth, C.K., 1922. A scale of grade and class terms for clastic sediments. J. Geol. 30 (5), 377–392.
- Wong, A.M., Campagnoli, J.G. and Cole, M.A., 2007. Assessing 155 years of hydrographic survey data for high resolution bathymetry grids. In OCEANS 2007 (pp. 1-8). IEEE.
- Woodgate, R.A., Aagaard, K., Weingartner, T.J., 2005. A year in the physical oceanography of the Chukchi Sea: Moored measurements from autumn 1990–1991. Deep Sea Res. Part II 52 (24–26), 3116–3149.
- Woodgate, R.A., Stafford, K.M., Prahl, F.G., 2015. A synthesis of year-round interdisciplinary mooring measurements in the Bering Strait (1990–2014) and the RUSALCA years (2004–2011). Oceanography 28 (3), 46–67. https://doi.org/10.5670/oceanog.2015.57.
- Woodgate, R. A., J. Johnson, A. Nguyen, M. Sonnewald, and B. Irving. 2016. Bering Strait Norseman II 2016 Mooring Cruise Report, 84 pp, University of Washington. http://psc.apl.washington.edu/HLD/Bstrait/BeringStrait2016CruiseReport_Norseman2_9thAugust2016wEL.pdf.
- Woodgate, R.A., 2018. Increases in the Pacific inflow to the Arctic from 1990 to 2015, and insights into seasonal trends and driving mechanisms from year-round Bering Strait mooring data. Prog. Oceanogr. 160, 124–154.
- Zhang, J., Steele, M., Lindsay, R.W., Schweiger, A., Morison, J., 2008. Ensemble one-year predictions of arctic sea ice for the spring and summer of 2008. Geophys. Res. Lett. 35, L08502. https://doi.org/10.1029/2008GL033244.
- Zhang, J., Woodgate, R., Moritz, R., 2010. Sea ice response to atmospheric and oceanic forcing in the Bering Sea. J. Phys. Oceanogr. 40 (8), 1729–1747.

- Zimmermann, M., and Benson, J. L., 2013. Smooth sheets: How to work with them in a GIS to derive bathymetry, features and substrates. U.S. Department of Commerce, NOAA Technical Memorandum NMFS-AFSC-249, 52 p.
- Zimmermann, M., Prescott, M.M., 2018. Bathymetry and Canyons of the Eastern Bering Sea Slope. Geosciences: Special Issue Marine Geomorphometry 8 (5), 184. https://doi.org/10.3390/geosciences8050184.
- Zimmermann, M., Ruggerone, G.T., Freymueller, J.T., Kinsman, N., Ward, D.H., Hogrefe, K., 2018. Volcanic ash deposition, eelgrass beds, and inshore habitat loss from the 1920s to the 1990s at Chignik, Alaska. Estuar. Coast. Shelf Sci. 202, 69–86. https://doi.org/10.1016/j.ecss.2017.12.001.
- Zimmermann, M., De Robertis, A., Ormseth, O. 2019a. Verification of historical smooth sheet bathymetry. Deep Sea Research Part II: Topical Studies in Oceanography: Understanding Ecosystem Processes in the Gulf of Alaska: Vol. 2. 165:292-302. https://doi.org/10.1016/j.dsr2.2018.06.006.
- Zimmermann, M., Prescott, M.M., Haeussler, P.J., 2019b. Bathymetry and Geomorphology of Shelikof Strait and the Western Gulf of Alaska. Geosciences: Special Issue Geological Seafloor Mapping. 9 (10), 409. https://doi.org/10.3390/geosciences9100409.
- Zimmermann, M., Prescott, M.M., 2021a. Passes of the Aleutian Islands: First detailed description. Fish. Oceanogr. 30 (3), 280–299. https://doi.org/10.1111/fog.12519.
- Zimmermann, M., Prescott, M.M., 2021b. False Pass, Alaska: Significant changes in depth and shoreline in the historic time period. Fish. Oceanogr. 30 (3), 264–279. https:// doi.org/10.1111/fog.12517.
- Zimmermann, M., Erikson, L.H., Gibbs, A.E., Prescott, M.M., Escarzaga, S.M., Tweedie, C. E., Kasper, J.L., Duvoy, P.X., 2022. Nearshore bathymetric changes along the Alaska Beaufort Sea coast and possible physical drivers. Cont. Shelf Res. 242, 104745 https://doi.org/10.1016/j.csr.2022.104745.